Islamic Azad University

Journal of
Optoelectronical Nanostructures

Winter 2024 / Vol. 9, No. 1

Research Paper

High-Performance Biosensor by using Au Nanoparticles and Grating for Sensing Waterborne Bacteria in Drinking Water

Shima Pirhaghshenasvali [1], Rahim Ghayour *[,1], Mahsa Vaghefi [1]

[1] Department of Electrical Engineering, Shiraz Branch, Islamic Azad University, Shiraz, Iran

Received: 3 Nov. 2023
Revised: 26 Nov. 2023
Accepted: 5 Dec. 2023
Published: 15 Mar. 2024

Use your device to scan and read the article online

Keywords:
Biosensor, Plasmonic, Escherichia Coli (E. coli) Bacteria, Nanoparticle

Abstract:

Water is an urgent human need; however, many people have difficulties gaining access to the safe and clean drink water. One of the most innovative techniques to solve this problem is known as biomolecular detection method. This can be followed through monitoring subtle changes in the refraction indices. In the present study, based on synthesis of gold nanoparticles (Au-NPs) on a grating structure sensor is proposed. The proposed structure operates as a refractive index (RI) sensor for detection of waterborne bacteria. Afterwards, we proceed with a cleverly designed RI biosensor optimized for waterborne diseases caused by Escherichia coli (E. coli) pathogen. This bacterial pathogen of various concentrations would be detectable by the proposed biosensor. Hence, the present study would lead to the development of plasmonic sensor with a sensitivity of as high as 467.1 nm/RIU (refractive index unit), in near-infrared region (NIR). In fact, the structure is capable of detecting a single bacterium contamination and determining the concentration level of bacterial spectrum in drinking water, as well.

Citation: Shima Pirhaghshenasvali, Rahim Ghayour *, Mahsa Vaghefi. High Performance Biosensor by using Au Nanoparticles and Grating for Sensing Waterborne Bacteria in Drinking Water. **Journal of Optoelectronical Nanostructures. 2024; 9 (1): 16- 36. DOI: 10.30495/JOPN.2024.32587.1303**

***Corresponding author:** Rahim Ghayour
Address: Department of Electrical Engineering, Shiraz Branch, Islamic Azad University, Shiraz, Iran. **Tell:** 00989177055393 **Email:** rghayour@shirazu.ac.ir

1. INTRODUCTION

Nowadays, waterborne health hazard is recognized as a severe environmental problem that afflicting human modern society. It is notably valuable to reinforce and regulate quality controls over drinking water in the regions surrounded by limited economic resources. This disaster is owing to the absence of effective treatment of the source water on the one hand, and the relatively considerable distance between production stations and the public consumer's taps on the other hand. Therefore, in certain cases, drinking water might be the origin of specific diseases among human beings. During last decade, a considerable increase in the number of sensing techniques created, while optical techniques with robust, inexpensive and reliable potentials recognized as a means for detecting infected biological materials [1]. In this respect, the most reliable and robust technique used to monitor subtle changes by precise optical spectrum of the material under test. In fact, the wavelength of any resonant peak corresponds to a testing germ can be inspected in response to the incidence of optical light. It is evident that monitoring any slight shift in resonant peak and subtle change in spectral width would be notably advantageous of optical techniques. As an interesting case, typical bacteria such as E. coli possess unique biophysical behavior by virtue of their refractive index and morphological properties. A single bacterium refractive index and its changes due to bacterium concentration are described in detail [2-4]. Impure water exhibits approximately higher refractive index value than that of the tap water. Nowadays, nanomaterials attract considerable interest in multiple applications consisting of electronics, biomedicine and sensing technologies on the strength of their specifically remarkable electronic, optical, catalytic and biological attributes [5, 6]. Furthermore, plasmonic sensors which functioning in accordance with the interaction of electrons and optical waves, have recently emerged as favorably convenient sensors for biological sensing [7, 8]. Multiple nano-sized metal structures demonstrate plasmonic properties and form a region of high light intensity [9]. Generally, metal-based nanoparticle preparation requires the synthesis of compounds that are toxic in essence [10, 11]. Mostly, metals reflect the energy of the incident beam through surface illumination; nevertheless, the absorbed light is emitted by means of vibrating free surface electrons. Surprisingly, noble metals possess truly unique features; such as they are convenient for plasmonic wide-ranging applications. Taking into account the electrical and optical properties stem from the large number of free electrons,

while noble metals play a more crucial role in plasmonic applications than dielectric ones [12,13]. Among all metals, gold (Au), silver (Ag), copper (Cu), and aluminum (Al) are commonly employed as plasmonic materials, meanwhile Au and Ag are the most common materials utilized surface plasmon in nanosensors. Interestingly, Au and Ag create resonance in surface plasmons at wavelengths within the visible range of the electromagnetic spectrum and provide narrow resonant peaks in the desired wavelengths range [14, 15]. Nowadays, to improve the performances of nanosensors, in the gain-assisted refractive index approach the metallic nanoscale slot and geometrical grating are implemented [16, 17]. Wang et al. have investigated the lattice plasmon of single and multiple Au nanoparticles and their related periodic arrangement [18]. Based upon this study, it became evident that the implementation of periodic patches of Au nanoparticles produces narrower resonant peaks than those by a single patch of Au nanoparticles [19]. Robust and narrow resonant peaks of plasmons in sensors using periodic patches of Au nanoparticles are noticeable. This is due to the coupling between plasmonic lattice resonances of Au nanoparticles and Bragg modes created by patch periodicity. In recent years, the synthesis of Au-NP arrays is among the most leading research projects and still is widely used in the field of nanotechnology. In this paper, a plasmonic biosensor is proposed which is based on combination of the periodic arrays of Au-NPs and the silicon nitride (Si3N4) grating surface, where they are placed on a thin layer of Au and silicon dioxide (SiO2) substrate. The proposed structure exhibits a high sensitivity of 467.1 nm/ RIU, which shows a significant improvement in this type of nanosensor. In fact, the current investigation proposes that bacterium sensing based on refractive index and plasmonic behavior might provide an efficient and alternative technique for identifying bacterial spectrum and determining the volume rate of concentration in the treated water sources. The proposed structure can function as a convenient optical device that provides the spectrum of the bacteria present in the drinking water. Single bacterium refractive index and the change in refractive index (determined by the E. coli volume rate of concentration) provide a solid basis for designing label-free and low-cost RI biosensors.

2. NUMERICAL ANALYSIS AND SIMULATION METHOD

Absorption is defined as a process in which the energy of a photon equals or outweighs the bandgap of the material under investigation. Coincidently, the material attracts the photon and excites an electron into the conduction band. Hence, photons incident on the surface of the semiconductor either reflected from the upper surface or absorbed onto the material. However, in frequent cases, both processes fail and the incident light transmits across the material under test. Since unabsorbed photons fail to produce power, reflection and transmission are generally considered as "loss mechanisms" of the optical sensors. Once a photon is absorbed, it develops a potential to excite an electron from the valence band into the conduction band and consequently produce electronic current within the device [20].

In order to boost the absorption rate, A, it is imperative to reduce the values of both transmission, T, and reflection, R, where A =1 − R − T. The reflectivity factor in an optical sensor operating at a frequency ω is [21, 22]:

$$\mathbf{R} = \frac{(\omega-\omega_0)^2}{(\omega-\omega_0)^2 + \frac{\Gamma^2}{4}} \quad (1)$$

where Γ and ω_0 are the bandwidth and resonant wavelength, respectively. In order to maximize the absorption rate (expressed as α), the reflection value must approach zero; hence, reflectivity turns zero at $\omega = \omega_0$.

Moreover, electron density within the device and resonant wavelength can be interrelated by [23]:

$$\lambda = \frac{c\sqrt{\varepsilon_0 \varepsilon_1 m_e}}{\sqrt{n_e e^2}} \quad (2)$$

where n_e is the electron density, e is the electronic charge, m_e is the effective mass of electron, ε_0 is the permittivity of free space, ε_1 is the permittivity of sensing medium and c is the speed of light. The electromagnetic field behaviors of the nanofeature devices are investigated through various multiple numerical methods such as multiple-multiple [24], Green's dynamic [25, 26], and finite difference time domain (FDTD) methods [27]. Moreover, FDTD method is a reliable way in solving Maxwell's equations in complex geometries and dispersive media such as Au and Ag. In order to study the performance of the

currently proposed sensor, the FDTD full wave-vector method is employed to solve the Maxwell equation.

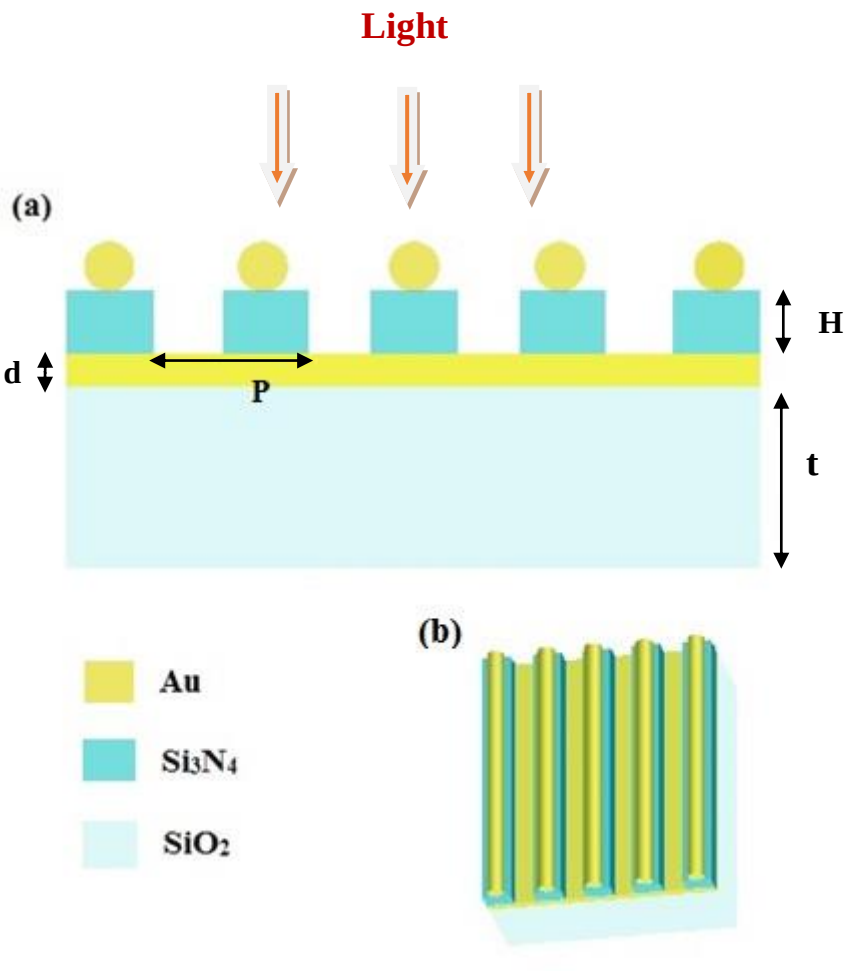

Fig. 1: (a) The unit cell of the structure, (b) The perspective of the biosensor structure.

In FDTD simulation, we can calculate the reflection and transmission spectra through setting two-dimensional power monitors that cover the structure. The underlying principle of the power monitor is the basis of the normalized surface integration of the Poynting flux densities. We calculate the normalized absorption rate (A) by acquiring reflectivity monitor data (R), transmittance monitor data (T) and applying A=1-R-T. The perfect matching layer (PML) as the boundary layer is selected in the y-direction to study the transmission and reflection properties of the electromagnetic field at normal incidence. Herein, an unpolarized light consisting of a plane electromagnetic wave in the wavelength range of 700 nm to 1200 nm is applied. It should be declared that, we proceed the work by investigating the dependence of the operation of our proposed structure on the material, diameter of NPs and the grating periodicity. In addition, the effects of geometrical parameters of the structure are investigated in detail. As illustrated in Fig. 1(a) the proposed biosensor is composed of periodic Au-NP arrays that are placed over a silicon nitride (Si_3N_4) rectangular grating and both sited on a thin Au layer and SiO_2 substrate. Therefore, the phase matching of generated plasmons has to be achieved by using a surface grating and NPs. The 3D schematic of the proposed biosensor is shown in Fig. 1(b).

3. RESULTS AND DISCUSSION

This section is focused on design and analysis of nanoscale biosensor based on the grating and using NP of different materials and sizes. The effects of device geometry and material types are investigated in detail. In this work, the main purpose is to design the most appropriate biosensor to distinguish different bacteria from each other.

(3-1) Effects of array of NPs and grating

In order to obtain some insight into the physical phenomena underlying the observed absorption peak, comparison between the presence and absence of the grating structure and NP arrays can be informative. First, we should check the effect of presence of grating on the performance of optical nanosensor. The absorption intensities and reflection spectra of sensor without Si_3N_4 grating layer and the presence of NPs are calculated and illustrated in Fig. 2(a). Additionally, the effect of implementing periodic arrays of NPs in biosensors is investigated by calculating the absorption and reflection spectra, where the result is compared with that of sensor without NPs, and the presence of grating as shown

in Fig. 2(b). observing the reflection spectra, by applying grating or NPs, the intensity of resonance varies significantly. Furthermore, as Fig. 2(c) shows, in presence of the grating structure and NP arrays, a maximum (peak) of absorption rate is achieved. By comparing Fig. 2(a), (b) and (c), it is obvious that by applying NPs and grating together into the structure, a more intense peak with a significant absorption enhancement in the NIR region is obtained. This phenomenon occurs due to the excitation of guided-mode resonances. It is noticeable that the peak in absorption spectrum corresponds to the suppression of the scattered surface plasmon modes from the Au-NPs and hence enhancement of the localized electric field at the resonant wavelength. Therefore, due to NPs arrays contribution on the surface plasmon resonance properties of the sensor by calculating the reflection spectrum of the nanostructures as shown in Fig. 2(d), the reflection dip at the interface of the Au NPs and substrate is happened.

Without grating

(a)

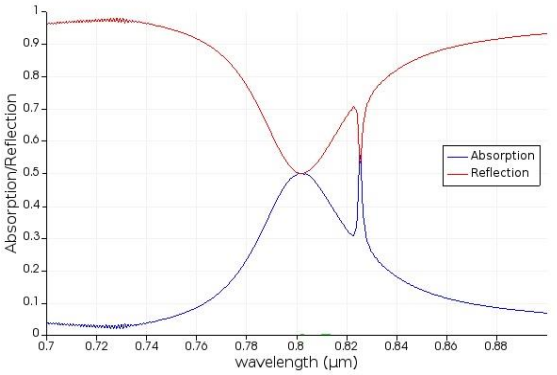

Without NPs

(b)

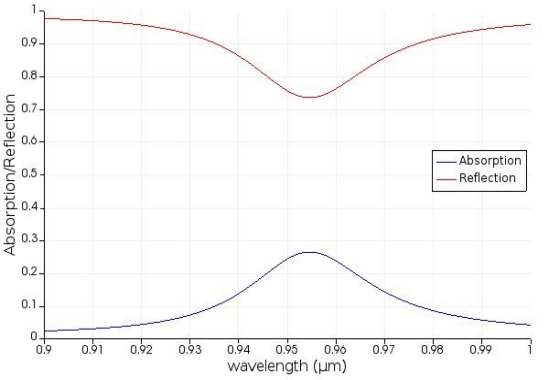

(c) **With NPs and grating**

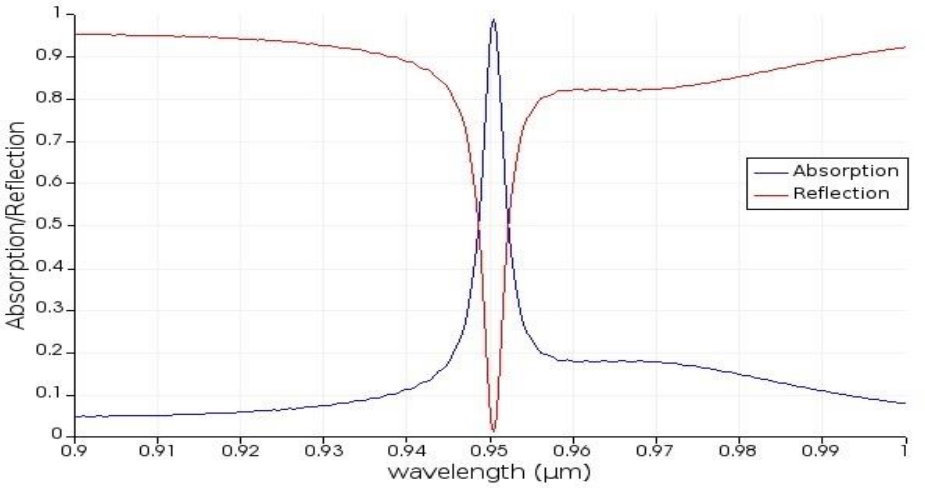

(d)

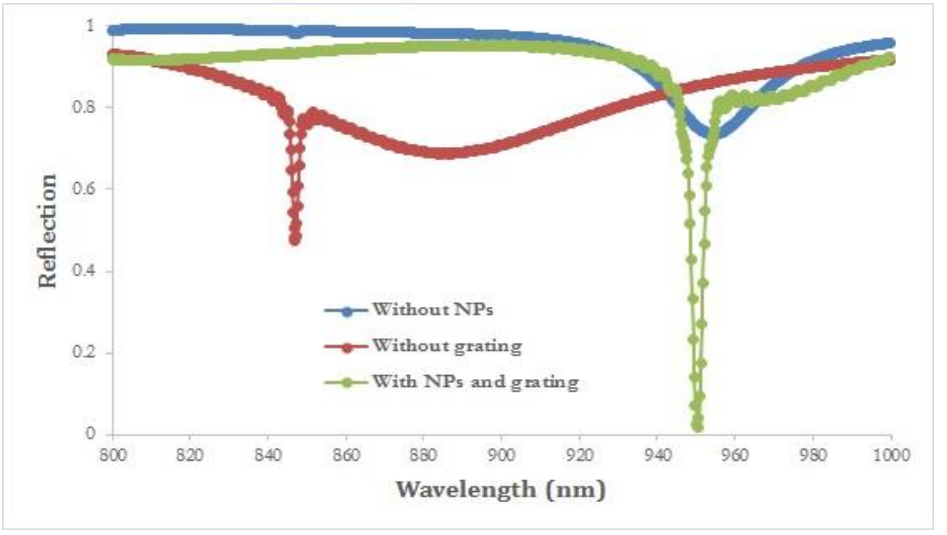

Fig .2: The calculated reflection and absorption spectra of the proposed structure: (a) without the grating structure, (b) without NP arrays, (c) with NPs and grating structure, (d) the reflection spectra without NPs or grating structure and with both.

(3-2) Effect of gold film

Now we compare the reflection spectra of the optimal structure of NPs, grating and gold film with the same geometry without gold film. As it is evident from Fig. 3(a), by employing a thin layer of Au between the SiO_2 substrate and the grating structure, the resonance mode is changed completely. Meanwhile, two plasmonic modes in the reflection function is achieved, where one of them can be used as a reference. The two resonances are excited within the two metal interfaces, where one of them is a long range SPR. Furthermore, with Au thin film two narrow reflection dips is achieved. One dip is sensitive to the refractive index (RI) of the cover media with a sensitivity of 467.1 nm/RIU and hence, the other is sensitive to the RI of the substrate. To investigate the effect of the thickness of metal film, the spectral responses of the sensor for different values of the metal thin film are shown in Fig. 3(b). As it is seen, the dependence of the resonant wavelength and right side dip to the thickness of the metal film is negligible. Our results show that the optimal thickness of metal film with lower reflection dips is obtained as 120 nm. The data presented in Fig. 3(b) is very important because it illustrate the vital role of the metal film thickness in order to allow physically excitation of two plasmons, everyone on each interface.

(a)

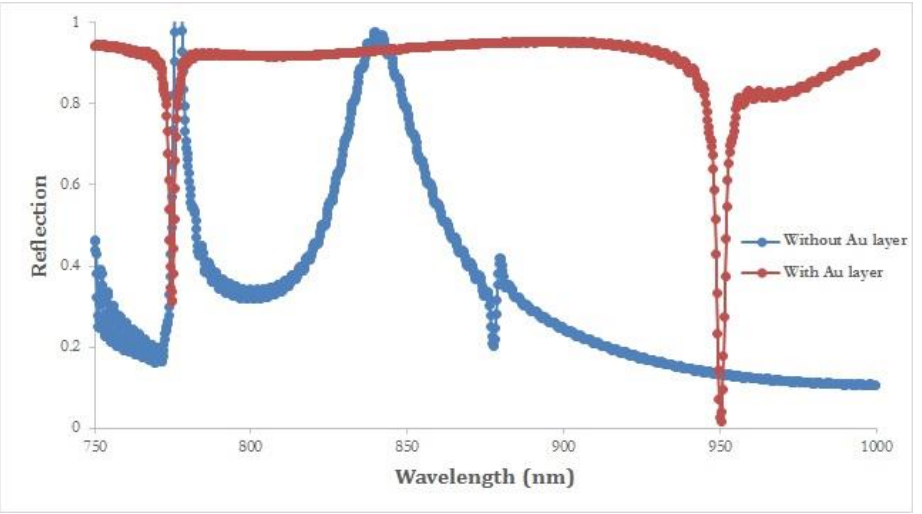

(b)

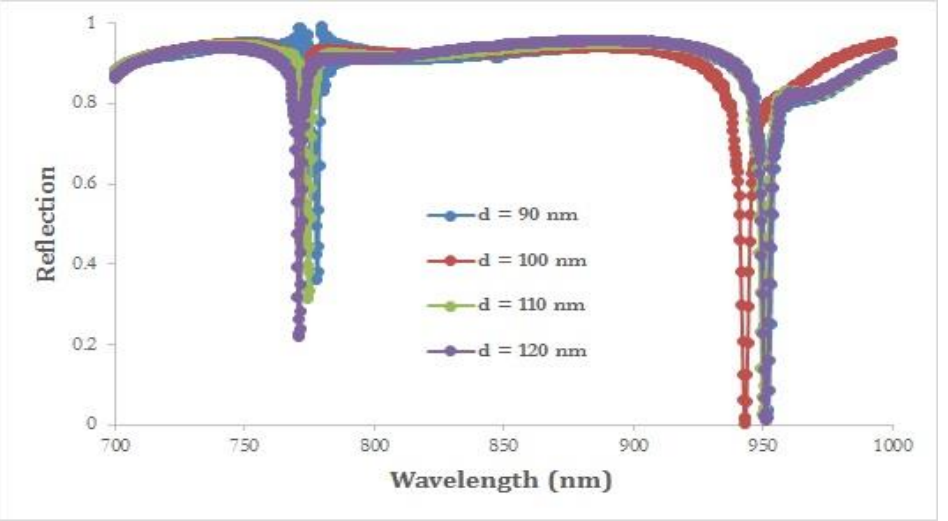

Fig. 3: The calculated reflection spectra (a) with and without the Au film and (b) for different values of "d" between 90 nm and 120 nm at n = 1.33.

(3-3) Effects of materials and size of NPs

The most used NP substances as: silver (Ag), gold (Au), copper (Cu), aluminum (Al), and chromium (Cr) are used to improve the reflection spectrum of biosensor. In the following, we present the performances of five types of NP biosensors. Now, we focus on the reflection characteristics of the proposed structure using different metallic materials while keeping other parameters constant. The results are shown in Fig. 4, where we can see that the Au-NPs can obtain lower reflection dip and significant linewidth reduction than those of Ag, Cu and Al NPs. Therefore, material type of NPs because of different plasmonic properties to evaluate of the biosensor performance are very important factor.

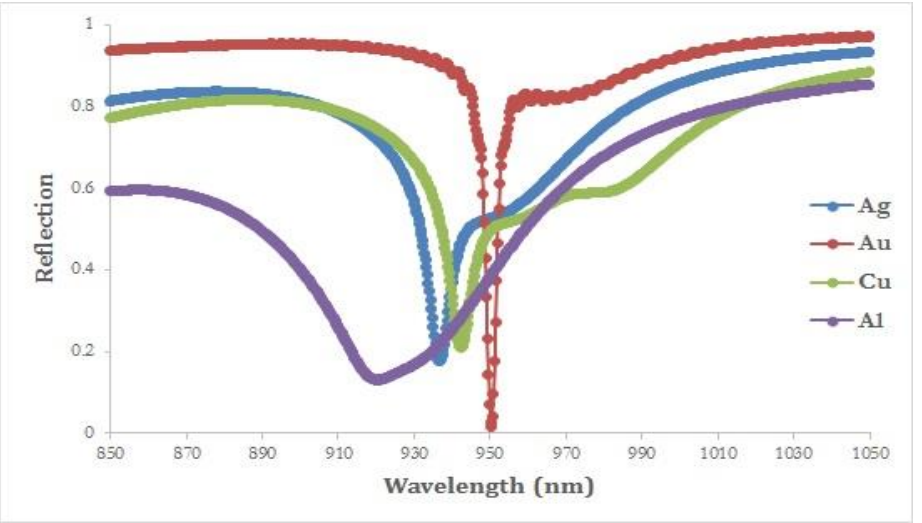

Fig. 4: The calculated reflection spectra of the sensors with metallic particles of: Ag, Au, Cu and Al.

Moreover, changing the radius (r) of an equal volume sphere of NPs is applied to characterize the effect of size of NPs on the reflection rate. The 'r' size is defined as:

$$r = (3V/4\pi)^{1/3} \quad (3)$$

where V is the volume of one NP.

To optimize the parameters, analyzing the effects of changes in Au NPs diameter on the surface plasmon properties of the nanostructure are useful. The results of optical response of biosensor for different radius (r) of Au NPs from 70 to 100 nm are calculated and shown in Fig. 5(a). As can be seen, by varying "r", shifts in the resonant wavelengths correspond to different sizes of NPs are happened.

It is considerable that the sensitivity is one of the main qualifications of biosensors that is calculated as follows [28]:

$$S = \frac{\Delta\lambda_{res}}{\Delta n_a} \quad (4)$$

where $\Delta\lambda_{res}$ shows the resonant wavelength due to the analyte refractive index change of Δn_a. Therefore, variations of the resonant wavelength versus different analyte refractive indices for different values of "r" are also determined and illustrated in Fig. 5(b). Based on equation 4, the slopes of the lines in Fig. 5(b) show the sensitivity of structure. The sensitivity of as high as 467.1 nm/RIU at the optimized size of r = 100 nm is obtained. Regarding the rate of sensitivity, the highest sensitivity can be achieved for the largest radius. Therefore, as it is evident, the resonance peak intensity and wavelength and also the rate of sensitivity depend on the size of NP diameter.

(a)

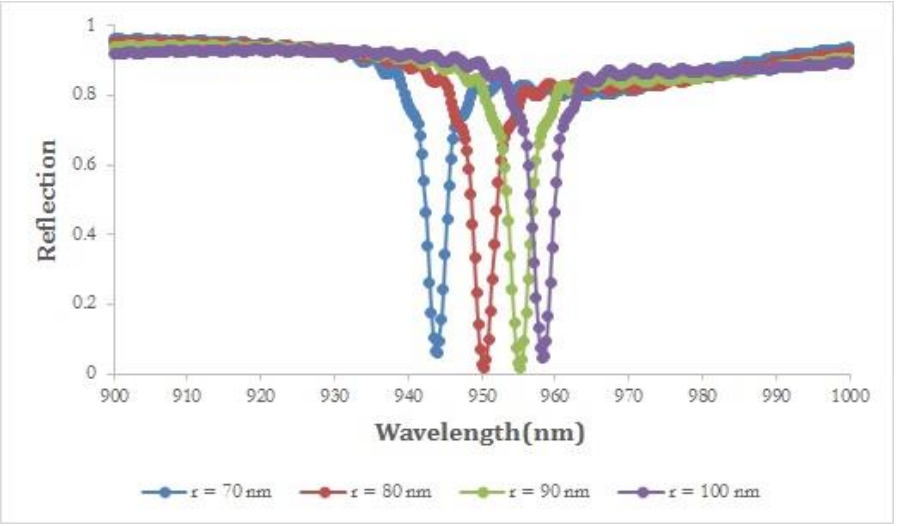

(b)

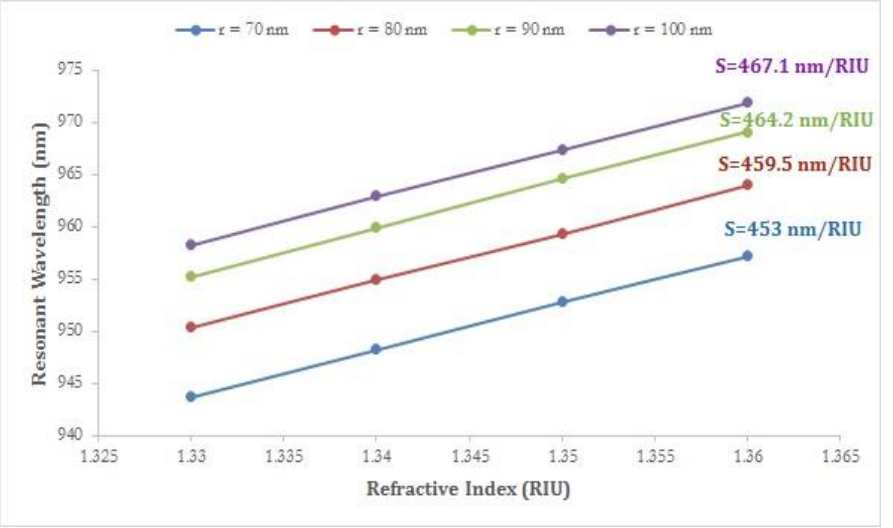

Fig. 5: (a) The reflection spectra for different values of "r" at n = 1.33, (b) variations of the sensitivity for different values of "r".

(3-4) Effect of grating periodicity

However, the periodicity (P) of grating is another important parameter to optimize the performance of a biosensor and adjust the resonance wavelengths. The reflection spectrum of normal incidence of TE-polarized light with different values of "P" is calculated and shown in Fig. 6. It is noteworthy that by increasing "P", the reflection spectra are shifted toward larger wavelengths and there are no significant changes in the recorded reflection intensity of each resonance wavelength at different grating periodicities.

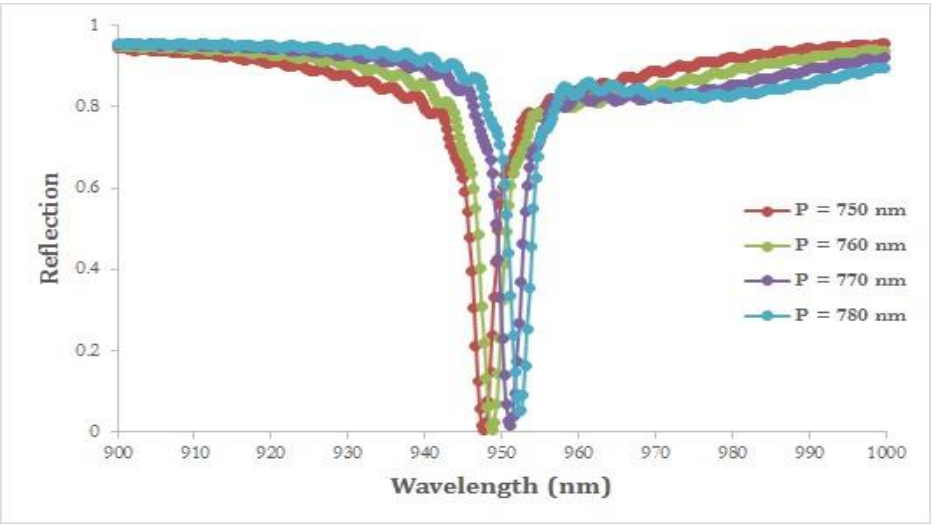

Fig. 6: The calculated reflection spectra different periodicity (P) at r = 80 nm.

In order to achieve a better insight into the performance of biosensor, the reflection spectra of the proposed biosensor applying different refractive indices from 1.33 to 1.36 under y-polarized (incident angle of 0°) light in near-infrared region are calculated and shown in Fig. 7. As it is shown, by increasing the analyze refractive index, considerable wavelength shifts due to phase matching between the incident wave and the resonances of excited guided modes are happened while that is suitable for sensing applications.

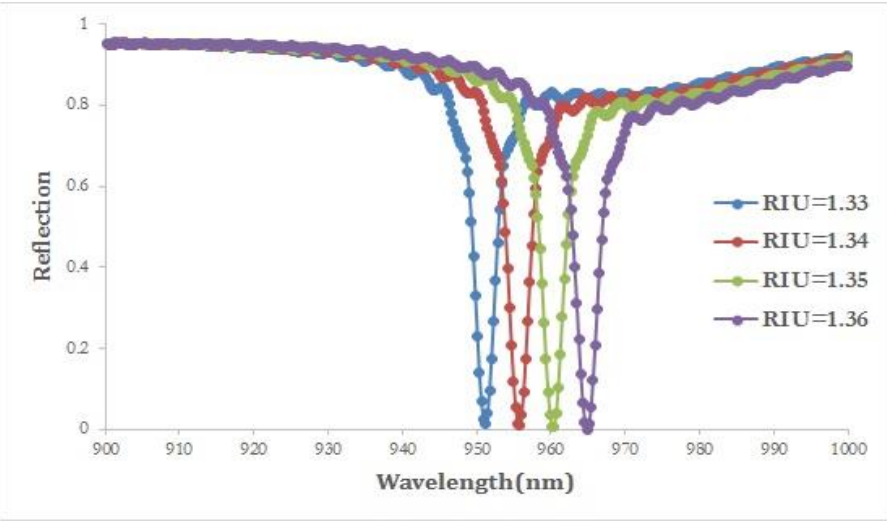

Fig. 7: Reflection spectra of our biosensor for refractive indices between 1.33 and 1.36, r = 80 nm.

These results emphasize the importance of plasmonic role in the optimization of NP configuration for biosensor applications. It is noteworthy that by utilizing plasmonic coupling between NPs, the phase matching between the incident wave and the excited guided mode resonance is happened, which causes a significant augment of surface sensitivity. Optimum parameters of the nanostructure are achieved under the highest absorption intensity and sensitivity, which are obtained by changing the bacterial concentration and consequent refraction indices. All geometrical parameters are optimized and obtained as: grating period of P = 770 nm, grating height of H = 200 nm, Au thin film thickness of d = 120 nm and SiO_2 thickness of t = 900 nm with Au-NP radius of 100 nm. Optimal parameters can be helpful to produce extremely narrow reflection spectra.

4. SENSOR PERFORMANCE

The sensing performance of the biosensor is the basis of detecting the E. coli bacterium in drinking water. It is worth noting that a change in refractive index due to growth of bacterium concentration leads to shifts in resonant wavelength and reflection intensity. Therefore, the variations of the reflection spectra in response to the various E-coli bacterium concentrations of single molecule, 1 CFU/ml, 2 CFU/ml and 3 CFU/ml are determined and presented in Fig. 8. In fact, a change in bacterium concentration appears as a change in refractive index of the solution under test. Furthermore, the sensitivity characteristics of different bacterium concentrations are indicated in Fig. 8. The sensitivity as high as 438.6 nm/RIU for single molecule (S. M.) E. coli bacteria is achieved. In addition, the sensitivities of 288 nm/RIU ,317 nm/RIU and 312 nm/RIU for 1 CFU/ml, 2 CFU/ml and 3 CFU/ml E. coli bacteria, respectively, are calculated. It is obvious that the extracted sensitivity can be one of the ways to distinguish concentration of different bacteria from each other. To clarify more, the refractive indices of different bacterial concentrations are given in Table 1. Moreover, the refractive index of pure drinking water is taken as 1.33 and further change in the refractive index due to bacterial growth is 0.184 per CFU/ml. The calculated resonant wavelength and sensitivity of all concentrations are summarized in Table 1. As detailed in this table, a change in refractive index due to growth of bacteria concentration leads to observable shifts in resonant wavelength and reflection spectra, while all the optimized parameters are applied.

Table 1: Refractive index, resonant wavelength and sensitivity of different E. coli bacterium concentrations

Concentration	E. coli Refractive index	Resonant wavelength (nm)	Sensitivity (nm/RIU)
Single molecules	1.401	982.942	438.6
1 CFU/ml	1.585	1029.34	288
2 CFU/ml	1.769	1079.29	317
3 CFU/ml	1.953	1134.34	312

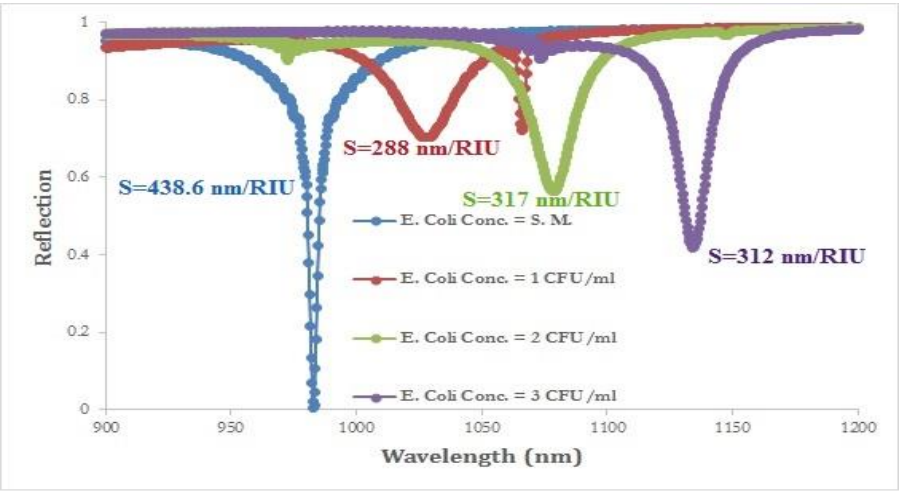

Fig .8: The calculated reflection spectra of various concentrations of E-coli bacterium.

Consequently, in Table 2 we compared the performance of few previous works and the results of our designed device. We obtained a significant improvement of the optical nanosensor performance and applications. The sensitivity of as large as 470.3 nm/RIU for the sensor is obtained. Therefore, the proposed structure is offering multiple advantages; such as higher sensitivity and an easier process to fabricate.

Table 2: Comparison between the performance of our proposed structure and the previous reported sensors

Reference	λ (nm)	S (nm/RIU)
[29]	986	294
[30]	1162	223
[31]	1536	190
[32]	1100	250
Proposed structure	950	467.1

5. CONCLUSION

In summary, the effects of Au nanoparticles (Au-NPs) on a Si_3N_4 grating substrate-based in all-optical plasmonic systems for sensing of the bacteria in the drinking water are assessed. The results confirm that the resonant properties

of absorption and reflection strongly depend on the material and also the geometrical parameters of NPs and grating structure. The bacterial pathogen namely Escherichia Coli in different concentrations can be detected by the proposed biosensor. The results for refractive index variations due to growth of concentrations of E. coli clearly indicate shifts in resonant dip wavelengths. In conclusion, this biosensor presented 467.1 nm/RIU maximum sensitivity rate at room temperature for detecting E-coli bacterium in drinking water.

REFERENCES

[1] Liu PY, Chin LK, Ser W, Chen HF, Hsieh M, Lee H (2016) Cell refractive index for cell biology and disease diagnosis: past, present and future. Lab Chip 16:634–644. https://doi.org/10.1039/C5LC01445J

[2] Liu PY, Chin LK, Ser W, Ayi TC, Yap PH, Bourouina T, Leprince-Wang Y (2014) An optofluidic imaging system to measure the biophysical signature of single waterborne bacteria. Lab Chip 14: 4237–4243. https://doi.org/10.1039/C4LC00783B

[3] Coles HJ, Jennings R,Morris VJ (1975) Refractive index increment measurement for bacterial suspensions. Phys Med Biol 20:310–313. https://doi.org/10.1088/0031-9155/20/2/013

[4] Bateman JB, Wagman J, Caratensen EL (1966) Refraction and absorption of light in bacterial suspensions. Colloid Polym Sci 208:44–58. https://doi.org/10.1007/BF01499867

[5] Servatkhah, M., & Goodarzi, S. (2017). Interaction of Laser Beam and Gold Nanoparticles, Study of Scattering Intensity and the Effective Parameters. *Journal of Optoelectronical Nanostructures*, *2*(3), 25-38. https://dorl.net/dor/20.1001.1.24237361.2017.2.3.3.1

[6] Firoozi, A., & Mohammadi, A. (2016). Investigating Molecular Spontaneous Emission Rate Enhancement Close to Elliptical Nanoparticles by Boundary Integral Method. *Journal of Optoelectronical Nanostructures*, *1*(3), 27-34. https://dorl.net/dor/20.1001.1.24237361.2016.1.3.3.4

[7] Ozozco CA, Urbon C, Knight MW, Halas NJ et al (2014) Au nanomatryoshkas as efficient near-infrared photothermal tranducers for cancer treatment: Benchmarking against nanoshells. ACS Nano 6:6372. https://doi.org/10.1021/nn501871d

[8] Oh SY, Heo NS, Shukla S, Huh YS et al (2017) Development of gold nanoparticle aptamer-based LSPR sensing chips for rapid detection of

Salmonella typhimurium in pork meat. Sci Rep 7:10130. https://doi.org/10.1038/s41598-017-10188-2

[9] Gruhl, F.J., Rapp, B.E., Lange, K.: Biosensors for diagnostic applications. Adv. Biochem. Eng. Biotechnol. **133**, 115–148 (2013). https://doi.org/10.1007/10_2011_130

[10] 63. Kofke MJ, Waldeck DH, Walker GC (2010) Composite nanoparticle nanoslit arrays: a novel platform for LSPR mediated subwavelength optical transmission. Opt Express 18(8):7705–7713. https://doi.org/10.1364/OE.18.007705

[11 Wu M, Zhao X, Zhang J, Schalch J, Duan G, Cremin K, Averitt RD, Zhang X (2017) A three-dimensional all-metal terahertz metamaterial perfect absorber. Appl Phys Lett 111(5):051101. http://dx.doi.org/10.1063/1.4996897

[12] Li R, Wu D, Liu Y, Yu L, Yu Z, Ye H (2017) Infrared plasmonic refractive index sensor with ultra-high figure of merit based on the optimized all-metal grating. Nanoscale Res Lett 12(1):1. http://dx.doi.org/10.1186/s11671-016-1773-2

[13] Maier S A 2007 Plasmonics: Fundamentals and Applications (Springer). https://extras.springer.com/?query=978-0-387-33150-8

[14] Azimi, H., Ahmadi, S. H., Manafi, M. R., Hashemi Moosavi, S. H., & Najafi, M. (2021). Development a simple and sensitive method for determination low trace of nickel by local surface plasmon resonance of citrate capped silver nanoparticles. *Journal of Optoelectronical Nanostructures*, *6*(2), 23-40. https://doi.org/10.30495/jopn.2021.26382.1210

[15] Zoghi, M. (2018). Reflection Shifts in Gold Nanoparticles. *Journal of Optoelectronical Nanostructures*, *3*(1), 1-14. https://dorl.net/dor/20.1001.1.24237361.2018.3.1.1.2

[16] Mohebbifar, M. R., & Zohrabi, M. (2019). Influence of Grating Parameters on the Field Enhancement of an Optical Antenna under Laser Irradiation. *Journal of Optoelectronical Nanostructures*, *4*(4), 65-80. https://dorl.net/dor/20.1001.1.24237361.2019.4.4.5.9

[17] Yang WH, Zhang C, Sun S, Jing J, Song Q, Xiao S (2017) Dark plasmonic modes based perfect absorption and refractive index sensing. Nanoscale 9:8907–8912. https://doi.org/10.1039/C7NR02768K

18. Wang D, Yang A, Hryn AJ, Schatz GC, Odom TW (2015) Superlattice plasmons in hierarchical Au nanoparticle arrays. ACS Photonics 2(12):1789–1794. https://pubs.acs.org/doi/abs/10.1021/acsphotonics.5b00546

[19] Kittel C and McEuen P 1996 Introduction to Solid State Physics (New York: Wiley). https://en.wikipedia.org/wiki/Special:BookSources/978-1-119-45416-8

[20] Liu N, MeschM, Weiss T, HentschelM, Giessen H (2010) Infrared perfect absorber and its application as plasmonic sensor. NanoLetters 10(7)2342–2348. https://doi.org/10.1021/nl9041033

[21] YeYQ, Jin Y, He S (2010) Omnidirectional, polarization insensitive and broadband thin absorber in the terahertz regime. J Opt Soc Am B: Opt Phys 27(3):498–504. https://doi.org/10.48550/arXiv.0906.2137

[22] Park H, Kim, Ho J, Beresford R, Xu J (2011) Effects of electrical contacts on the photoconductive gain of nanowire photodetectors. Appl Phys Lett 99(14):143110. https://doi.org/10.1063/1.3647559

[23] S.A. Maier, Plasmonics: fundamentals and applications. 2007: Springer Science & Business Media. https://extras.springer.com/?query=978-0-387-33150-8

[24] Wannemacher R (2001) Plasmon supported-transmission of light through nanometric holes in metallic thin films. Opt Commun 195:107–118. https://doi.org/10.1016/S0030-4018(01)01333-5

[25] Cattoni A, Ghenuche P, Haghiri-Gosnet AM, Decanini D, Chen J, Pelouard JL, Collin S (2011) Lambda (3)/1000 plasmonic nanocavities for biosensing fabricated by soft UV nanoimprint lithography. Nano Lett 11(9):3557–3563. https://doi.org/10.1021/nl201004c

[26] Francs GC d, Molenda D, Fischer UC, Naber A (2005) Enhanced light confinement in a triangular aperture: experimental evidence and numerical calculations. Phys Rev B 72(16). http://dx.doi.org/10.1103/PhysRevB.72.165111

[27] Irannejad M, Cui B, Yavuz M (2015) Optical properties and liquid sensitivity of Au-SiO2-Au nanobelt structure. Plasmonics 11(1):1– 9. https://doi.org/10.1007/s11468-015-9977-3

[28] A. Rifat, M. Rahmani, L. Xu, and A. Miroshnichenko, "Hybrid metasurface based tunable near-perfect absorber and plasmonic sensor," Materials, vol. 11, no. 7, p. 1091, Jun. 2018. https://doi.org/10.3390/ma11071091

[29] Wei Z, Li X, Zhong N, Tan X, Zhang X, Liu H, Meng H, Liang R (2016) Analogue electromagnetically induced transparency based on low-loss metamaterial and its application in nanosensor and slow-light device. Plasmonics 12:641–647. https://link.springer.com/article/10.1007/s11468-016-0309-z

[30] Zhou P, Zheng G (2018) High-efficient light absorption of monolayer graphene via cylindrical dielectric arrays and the sensing application. Opt Mater 78:471–476. https://doi.org/10.1016/j.optmat.2018.02.060

[31] Lu X, Zhang L, Zhang T (2015) Nanoslit-microcavity-based narrow band absorber for sensing applications. Opt Express 23:20715–20720. https://doi.org/10.1364/OE.23.020715

[32] Chen, J. et al. Dielectric waveguide-enhanced localized surface plasmon resonance refractive index sensing. Opt. Mater. Express 8, 342–345 (2018). https://doi.org/10.1364/OME.8.000342